J Polym Res (2012) 19:9778
DOI 10.1007/s10965-011-9778-0

ORIGINAL PAPER

# Multiscale modeling of syndiospecific styrene polymerization

**S. R. Sultan · W. J. N. Fernando · Suhairi A. Sata**

Received: 22 May 2011 / Accepted: 10 October 2011 / Published online: 1 March 2012


**Abstract** A detailed mathematical model for syndiospecific styrene polymerization based on combining features of the multigrain model (MGM) and the polymeric multigrain model (PMGM). This model has been established to predict the radial monomer concentration within the growing macro particles and the rate of polymerization. The latter, the parameters, have an effect on the molecular weight distribution (MWD). In this model, the effect of intraparticle diffusion resistance and the radius of catalyst particles on the rate of polymerization and MWD were studied. The model simulation showed the presence of a large distribution of monomer concentration across the radius of particles. It was further noticed that the diffusion resistance was most intense at the beginning of the polymerization process. For MWD, the model simulation showed that the existence of diffusion resistance led to have an increase in the molecular weight within a period of time similar to the one needed in the catalyst decay. Moreover, the validation of the model with experimental data given a good agreement results and show that the model is able to predict a correct monomer profile, polymerization rate, particle growth factor and MWD, an algorithm, which embeds physicochemical effects, has been developed to model the industrial reactors.

**Keywords** Multiscale modeling · Particle growth · Multigrain model · Syndiospecific styrene polymerization · Mass transfer

S. R. Sultan · W. J. N. Fernando · S. A. Sata (✉)
School of Chemical Engineering, Universiti Sains Malaysia, 14300, Nibong Tebal, Penang, Malaysia
e-mail: chhairi@eng.usm.my

S. R. Sultan
Chemical Engineering Department, University of Technology, Baghdad, Iraq

## Nomenclature

| | |
|---|---|
| $D_{ef,i}$ | Effective macroparticle diffusivity, at the *i*th grid point ($cm^2.\ min^{-1}$) |
| $D_l$ | Monomer diffusivity in pure polymer ($cm^2.min^{-1}$) |
| $D_s$ | Effective microparticle diffusion coefficient ($cm^2.\ min^{-1}$) |
| $k_p$ | Propagation rate constant ($L.\ mol^{-1}\ .hr^{-1}$) |
| $k_d$ | Catalyst deactivation rate constant ($hr^{-1}$) |
| $k_{tM}$ | Chain transfer to monomer rate constant ($L.\ mol^{-1}\ .hr^{-1}$) |
| $k_{t\beta}$ | β—hydrogen elimination rate constant ($hr^{-1}$) |
| $k_l$ | liquid film mass transfer coefficient ($m^2.s^{-1}$) |
| $M_{M,\ i}$ | Monomer concentration in the macroparticle, at the ith grid point ($mol.dm^{-3}$) |
| $M_{\mu,i}$ | Monomer concentration in the microparticle, at the ith grid point ($mol.dm^{-3}$) |
| $M_b$ | Bulk monomer concentration ($mol.dm^{-3}$) |
| $M_n$ | Number average molecular weight ($g.mol^{-1}$) |
| $M_w$ | Weight average molecular weight ($g.mol^{-1}$) |
| $(mw)_{sty}$ | Styrene Molecular weight ($g.mol^{-1}$) |
| N | Number of shell |
| r | Radial position at the macroparticle level (m) |
| $r_s$ | Radial position at the microparticle level (m) |
| $R_c$ | Radius of catalyst subparticles (m) |
| $R_{N+2}$ | Macroparticle radius (m) |
| $R_o$ | Initial particle radius (m) |
| $R_{h,i}$ | Radius of ith hypothetical shells |
| $R_{s,i}$ | Radius of microparticle at ith hypothetical shells |
| $R_{pv,i}$ | Rate of reaction per unit volume at the ith grid point ($mol\ (m^3.s)^{-1}$) |
| $V_{cs,i}$ | Volume of the ith hypothesis shell |
| $V_{cc,i}$ | Volume of catalyst in shell i |

## Greek Letters

| | |
|---|---|
| β | Indicator of the monomer convection contribution |
| $\lambda_{Pk}$ | kth Moment of live polymers |
| $\lambda_{Mk}$ | kth moment of dead polymers |

## Introduction

Polystyrene is one of the most prominent and extensively used plastic polymers. In the United States, for instance, the production of styrene homopolymer approximately reaches two billion pounds. The typical application of polystyrene includes: food packaging, toys, appliances and compact disc cases [1].

There are three different stereo-isomers of polystyrene: atactic polystyrene (aPS), isotactic polystyrene (iPS) and Syndiotactic polystyrene (sPS). The abbreviation aPS refers to an amorphous polymer; it is one of the most widely used commodity polymers because of its good transparency, stiffness, and good processibility. In this type of polymer, the phenyl groups are in the aPS, and the polystyrene is randomly distributed to the main polymer backbone. As for iPS, it is a semi-crystalline polymer with a melting point of around 240 °C. Because of its very slow crystallization rate, iPS is less used to make injecting moldable objects; besides, it can be synthesized over Ziegler-Natta catalysts. In iPS, phenyl groups are found to be distributed on the same side of the backbone chain plane. Finally, sPS is semi-crystalline polystyrene, which can be prepared by stereoregular polymerization of styrene in synchronism with methylaluminoxane (MAO). sPS has a melting point of up to 275 °C with high crystallization rate while the iPS and aPS have a melting point of 240 and 100 °C, respectively. In sPS, phenyl groups alternate vertically along the backbone chain. The new property of sPS that is similar to those of some expensive engineering plastics paid the interest towards it [2–5].

Syndiotactic polystyrene was first synthesized by Ishihara [6], with cyclopentadienyl titanium trichloride ($CpTiCl_3$) catalyst. Since then, many different titanium compounds have been found active to produce sPS [7]. In particular, half sandwiched titanium compounds (e.g. CpTi- and Cp*Ti- complexes) have high polymerization activities and high Syndiospecificity. The kinetics of syndiotactic polymerization of styrene is composed of four steps, namely: catalyst site activation (initiation) step, propagation step, chain transfer (termination) step, and catalyst deactivation step. The Ti (III) cation is known as an active site of the catalyst for the syndiotactic polymerization of styrene. The catalyst site activation step embeds reducing the titanium of the oxidation state (IV) in the titanium complex to the oxidation state (III) with an aluminum alkyl, $AlR_3$ or MAO. Then, the Ti (III) complex is alkylated again by MAO or $AlR_3$, and finally the reaction with the cocatalyst will produce the active Ti (III) cation. The final step is an equilibrium reaction. Therefore, a larger amount of MAO promotes polymerization rate by making more active Ti(III) cations. The second step is a propagation step in which styrene monomers are converted to an syndiotactic polymer at the active cationic Ti(III) site. The propagation reaction at the active site is described by the stereo chemical control of the reaction and is understood by the cis-opening of the double bond of styrene. The secondary insertion into the Ti–carbon bond—benzylic carbon is then directly bonded to the Ti (III) ion—and the chain-end control of the insertion mechanism. When styrene monomer approaches the catalyst active center, syndiotactic configuration is favored because of the phenyl-phenyl repulsion between the last inserted unit of a polymer chain and the incoming monomer. The propagation reaction can be terminated by a species that contains an exchangeable proton. The main termination reactions in catalyzed polymerization are β-hydride elimination (abstraction) and chain transfer to monomer [2].

Despite the intensive research that has been conducted for many years, a great controversy remained with regard to several concepts of the polymerization process that range from the kinetic mechanisms to the growing morphology of the particles. The kinetic of polymerization is often masked by intraparticle, interfacial mass and by heat transfer limitations. The simplest type of model to describe this phenomenon is based on a spherical layer of polymer particle that is formed around the spherical catalyst particle. Models based on this geometry are commonly called solid core models (SCM). Monomer diffusion from the polymer shell to the active site on the catalyst surface is the central theme of these models.

Schmeal [8, 9] and Nagel et al. [10], used the SCM model for olefins polymerization over Ziegler-Natta catalysts. They concluded that with a single active site catalyst; this model could not predict the MWD. According to the solid core model, the monomer concentration is constant at the external surface of catalyst where the polymerization reaction occurs only at the surface. Thus, the polymer product has the same average properties in all chains; a conclusion that is inconsistent with experimental studies because the catalyst particles are porous fragments.

Singh [11] and Galvan [12, 13], proposed the polymeric flow model (PFM). This model supposes that the catalyst fragments and polymer chains grow form a continuum. Their supposition represents a big improvement in comparison to the previous models; for they do not agree with a large number of experiments in that they do not take into consideration the catalyst particle fragmentation.

In the last two decades, more papers have been published on the polymer particle growth modeling and morphology. However, most of these studies were based on the MGM of Floyd et al. [14], as shown in Fig. 1. Nagel et al. [10] and Floyd et al. [14–16] were the first to propose this model to estimate the yield of polymer product and MWD. In accordance with the numerous experiments, the MGM assumes a rapid breakup of the catalyst particles into small fragments, which are distributed throughout the polymer particles.

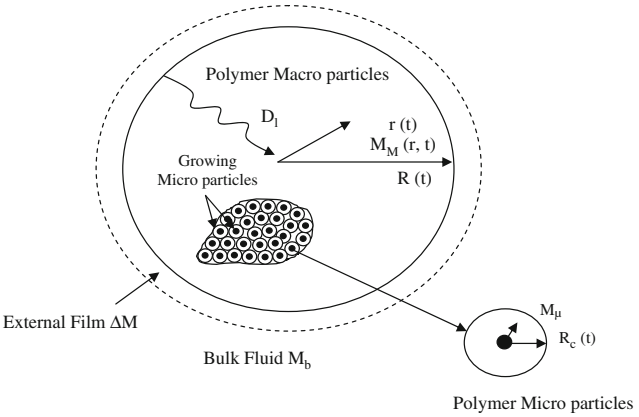


**Fig. 1** Schematic of MGM Model [14]

Thus, the large polymer particle (macro particles) will consist of many small molecules (micro particles), which encapsulate these catalyst fragments. For the monomer particles to reach the active sites, it must first be diffused through the pores of macro particles, between the micro particles, and then to micro particles themselves. In general, the diffusion resistances in both cases are not equal; besides, they include the possibility of having an equilibrium sorption of monomer particles at the surface of micro particle. The disadvantage of this model is that it is time consuming when using the computer to get results.

Hutchinson et al. [17], modified MGM the modeling of the particle growth and morphology in the copolymerization system. However, they found that one of the shortcomings of this modeling is the complexity of the equations and consequently the time consuming numerical computations when executing the program, which makes it inappropriate for polymerization process application.

Sarkar and Gupta [18, 19], derived a model called the polymeric multigrain model (PMGM) that combines features of the multigrain model with some features of the simplified polymer flow model. The authors observed a significant computational time reduction without any significant error increase of the results in PMGM model. They found that PMGM can predict the poly dispersity (PDI) values are higher than that of the multigrain model predictions with respect to the single site and deactivating catalysts.

The polymeric multilayer model (PMLM) was suggested by Soares and Hamielec [20]; it seems to be less complex than the previous models. In this model, the macroparticle is divided into concentric spherical layers as well as MGM and PMGM. The researchers further noticed that there is no presence of microparticle to simplify their model and that all layers of the growing particles have a similar concentration to that of the active sites at early step of polymerization.

Kanellopoulos et al. [21], developed a model that was called the random—pore polymeric flow model RPPFM it was based on the PFM because gas-phase olefin polymerization takes into account both the external and internal heat and mass transfer resistances. It has also been shown that both the particle overheating and polymerization rate increase when increasing the concentration of the initial catalyst size and active metal. It was further demonstrated that the monomer sorption kinetics greatly affects the polymerization rate and the particle overheating; especially; during the first few seconds of the polymerization.

Chen & Liu [22]and Liu [23] presented a modified model for single particle propylene polymerization over heterogeneous catalysts. This model is extended mainly from PMGM model and MGM model by taking the effect of monomer diffusion at both the macro- and microparticle levels. It has also been noticed that the model can give higher values of PDI, (PDI about 6–25).

Finally, Diffusion limited aggregation (DLA) model is developed by Kanellopoulos et al. [24], to calculate the transport of penetrated molecules in semi crystalline nonporous polyolefin films and porous powders in terms of the internal particle morphology of the polymer. The authors observed that the morphological characteristics of porous polyolefin particles can be described using the proposed DLA model in terms of the size distribution of the microparticles and the extent of microparticles fusion.

It is clearly noticed from the publications mentioned above that most of the models applied to the olefins polymerization use Ziegler-Natta catalysts in the gas and slurry phase. In this paper, a comprehensive mathematical model describing the particles growth for syndiotactic styrene polymerization system based on combining features from MGM and PMGM models to predict the polymerization rate, particle growth, and the effective parameters on MWD.

## Modeling of polymer particles growth

The radial gradients in the growth of polymer particles gives with the passage of time a distribution system for monomer concentration and for the rate of polymerization as a function of position and time. Thus, it is possible to get the physical properties of the polymer as a function of position and time. Consider Fig. 2, which shows the best description of the model with respect to the growing particles. As mentioned previously, MGM assumes a rapid breakup of the catalyst particles to small fragments which are distributed throughout polymer particles. This makes the large polymer particle (macro particles) consist of many small polymer particles (micro particles), as indicated in Fig. 2.

Furthermore, one can notice the hypothetical radius of macro particle shells that can be defined by ($Rh_i$) whereas the micro particle can be placed at the mid-point of each hypothesis shell. At time zero, it is assumed that there is no

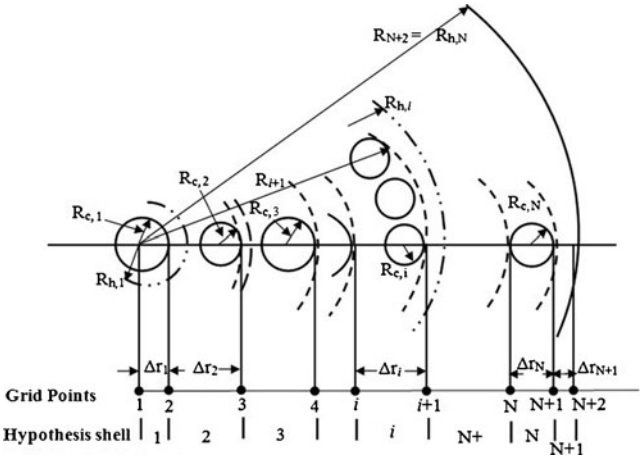


**Fig. 2** Schematic of PMGM model [18]

monomer diffusion toward the catalyst surface that is why the sizes of all shells are equal. Whenever the polymerization starts, all monomer particles diffuse and reach the active site on the catalyst surface. In fact, all the micro particles are surrounded by growing polymer chains. Therefore their size, volume and position change; accordingly, it is necessary to update all positions and volumes at any time interval.

All of the micro particles at a given macro particles radius are assumed to be similar in size and spherical. The macro particle of (N) shell is considered in this paper, where every shell has been filled out with ($N_i$) micro particles, which can be calculated by the following equation:

$$N_1 = 1 \tag{1a}$$

$$N_i = 24(1-\varepsilon)(i-1)^2 \qquad i = 2,3,\ldots..N \tag{1b}$$

Where (ε) is the porosity, which is thought to be a constant and ith is shell of macro particle.

In order to create a particles growing model, the relation between monomer concentration in the macro and micro particles must be developed. Accordingly, the diffusion equation for a single spherical macro particle monomer can be as follows:

$$\frac{\partial M_M}{\partial t} = \frac{D_{ef}}{r^2}\frac{\partial}{\partial r}\left(r^2\frac{\partial M_M}{\partial r}\right) - R_{Pv} \tag{2}$$

I.C. $M_M(r, t=0) = M_o = 0$

B.C.1 $\dfrac{\partial M_M}{\partial r}(r=0,t) = 0$

B.C.2 $D_{ef}\dfrac{\partial M_M}{\partial r}(r=R_p,t) = k_1(M_b - M_M)$

Where $M_M$ is the monomer concentration in the macroparticle; $D_{ef}$ is the effective diffusive of monomer; $R_{pv}$ is the volumetric rate of polymerization in the macroparticle; $M_o$ and $M_b$ are the initial and bulk monomer concentration, respectively and $k_1$ is the mass transfer coefficient.

This model combines features of MGM and PMGM models by assuming the catalyst fragments and polymer particles in a continuum. This model has also been used by Sarkar and Gupta [18, 19], they assumed that in PMGM, no porosity in the macro-particle exists; an assumption that is in contrast with what happens in MGM, [14–16].

The monomer concentration profile in the spherical micro particle is the same as that in SCM model:

$$\frac{\partial M_\mu}{\partial t} = \frac{1}{r^2}\frac{\partial}{\partial r}\left(D_s r^2\frac{\partial M_\mu}{\partial r}\right) \tag{3}$$

I.C. $M_\mu(r, t=0) = M_{\mu o} = 0$

B.C.1 $4\pi R_c^2 D_s\dfrac{\partial M_\mu}{\partial r}(r=R_c,t) = \dfrac{4}{3}\pi R_c^3 R_{Pc}$

B.C.2 $M_\mu(r=R_s,t) = [M]_{eq} = \eta_\mu^* M_M \le M_M$

Where $M_\mu$ is the monomer concentration in the micro particle; $D_s$ is the effective diffusivity of monomer in the micro particle; $M_{eq}$ is the equilibrium concentration of monomer; $M_{\mu o}$ is the initial monomer concentration in the micro particle; $R_{pc}$ is the polymerization rate at catalyst fragments surface; $R_c$ is the catalyst fragments radius in the micro particle; r is the radial position in the micro particle; and $R_s$ is the radius of the micro particle.

Using the quasi steady state approximation (QSSA) offered by Hutchinson et al. [17], ($M_\mu$) can be put as stated below:

$$M_\mu = \frac{\eta_\mu^* M_M}{1 + \frac{R_c^2}{3D_s}\left(1-\frac{R_c}{R_s}\right)k_p C^*} \tag{4}$$

Where $M_\mu$ is the monomer concentration at the catalyst surface in the micro particle; $k_e$ is the equilibrium constant of monomer absorption in the micro particle.

Equation (2) is converted to a set of (N+2) ordinary differential equations (ODEs) of monomer concentration at (i) position by using a finite difference technique that was stated by Finlayson [25], with regard to the unequally spaced grid points, as indicated below:

$$\frac{dM_{M1}}{dt} = D_{ef,1}\frac{(M_{M2}-M_{M1})}{(\Delta r_1)^2} - R_{pv,1} \tag{5a}$$

$$\frac{dM_{Mi}}{dt} = D_{ef,i}\left[M_{Mi+1}\left(\frac{1}{\Delta r_i R_i}+\frac{1}{\Delta r_i^2}\right) - M_{Mi}\left(\frac{1}{\Delta r_i^2}+\frac{1}{\Delta r_{i-1}\Delta r_i}\right) + M_{Mi-1}\left(\frac{1}{\Delta r_{i-1}\Delta r_i}-\frac{1}{\Delta r_i R_i}\right)\right] - R_{pv,i} \qquad i = 2,3\ldots\ldots\ldots\ldots,N+1 \tag{5b}$$

$$\frac{dM_{MN+2}}{dt} = -M_{MN+2}\left[\frac{k_1}{\Delta r_{N+1}} + \frac{D_{ef,N+2}}{\Delta r_{N+1}^2} + \frac{2k_1}{R_{N+2}}\right] + M_{MN+1}\left[\frac{2D_{ef,N+2}}{\Delta r_{N+1}^2}\right] + M_b\left[\frac{k_1}{\Delta r_{N+1}} + \frac{2k_1}{R_{N+2}}\right] - R_{pv,N+2} \quad (5c)$$

In the equations (5a, 5b & 5c), the subscript i ( i=1, 2..... N+1), on any variable, indicates its value at the ith grid point. The calculations of (Δr and R) at (ith) position are given in Appendix 1.

The effective diffusivity, ($D_{ef}$) is commonly estimated from monomer diffusivity in pure polymer ($D_1$), and as follows:

$$D_{ef} = D_1 \cdot \frac{\varepsilon}{\tau} \quad (6)$$

Where (ε) and (τ) are the porosity and tortuosity of the macro particle, respectively. According to the correction of Sarkar and Gupta [19], the effective diffusivity at (ith) position can be given as follows.

$$D_{ef,1} = D_{ef,N+2} = D_1 \quad (7a)$$

$$D_{ef,2} = D_1 N_1 \frac{R_c^3}{R_{h,1}^3} \quad (7b)$$

$$D_{ef,i+1} = D_1 \frac{(V_{cs,i} - V_{cc,i})}{V_{cs,i}} = D_1 \frac{R_{h,i}^3 - R_{h,i-1}^3 - N_i R_c^3}{R_{h,i}^3 - R_{h,i-1}^3} \quad (7c)$$

Where $D_1$ is the diffusion coefficient of monomer in pure polymer; Vcs,i and $V_{cc,i}$ are the volume of the ith shell and the catalyst volume in shell (i), respectively.

The volumetric rate of monomer consumption at any radial location, $R_{pv}$, can be calculated by:

$$R_{pv,1} = R_{pv,N+2} = 0 \quad (8a)$$

$$R_{pv,2} = \frac{k_p C^* M_{\mu,i} N_1 R_c^3}{R_{h,1}^3} \quad (8b)$$

$$R_{pv,i} = \frac{k_p C^* M_{\mu,i-1} N_{i-1} R_c^3}{\left(R_{h,i}^3 - R_{h,i-1}^3\right)} \quad (8c)$$

Where $R_{pv,1} = R_{pv,N+2} = 0$. So, the overall time-dependent reaction rate can be estimated as follow:

$$R_{overall} = \frac{k_p C^* (mw)_{sty} \sum_{i=1}^{N} (N_i M_{\mu,i})}{\rho_c \sum_{i=1}^{N} N_i} \quad (9)$$

Where $M_{\mu,i}$ is the monomer concentration in the micro particle at any radial position, as illustrated below:

$$M_{\mu,i} = \frac{\eta_\mu^* M_{M,i}}{1 + \frac{R_c^2}{3D_s}\left(1 - \frac{R_c}{R_{s,i}}\right) k_p C^*} \quad (10)$$

The rate of polymerization on the microparticles is generally given by:

$$R_{pc} = k_p(t) C^*(t) M_\mu \quad (11)$$

Where $k_p$ (t) is the constant propagation rate and $C^*$ (t) is the active sites concentration on the surface of the micro particle, which can be calculated from the kinetic reaction model as shown below:–

Catalyst activation:

$$C_o + MAO \xrightarrow{ka} C^*$$

Propagation:

$$C^* + M \xrightarrow{kp} P_1 \; ; \; P_n + M \xrightarrow{kp} P_{n+1}$$

Chain transfer to monomer:

$$P_n + M \xrightarrow{ktM} M_n + P_1$$

β-hydrogen elimination:

$$P_n \xrightarrow{kt\beta} M_n + C^*$$

Catalyst deactivation:

$$C^* \xrightarrow{kd} D^* \; ; \; P_n \xrightarrow{kd} D^*$$

Where $C_o$ is the potent catalyst site; C* is the activated catalyst site; $P_n$ and $M_n$ are the live and dead polymer chains of length n; M is the monomer; and D* is the deactivated catalyst site. As for $k_j$, it represents the reaction rate constant for each corresponding reaction. The method of moments is used to calculate the molecular weight and MWD and the polymerization rate; accordingly, the equations and moment equations are derived as follows:

$$\frac{dC^*}{dt} = -k_d C^* - k_p C^* M_\mu + k_{t\beta} \lambda_{po} \quad (12)$$

$$\frac{dM_\mu}{dt} = -k_p P M_\mu \quad (13)$$

$$\frac{dP_1}{dt} = k_p C^* M_\mu - k_p P_1 M_\mu - k_{tM} P_1 M_\mu + k_{tM} \lambda_{po} M_\mu - k_{t\beta} P_1 - k_d P_1 \quad (14)$$

$$\frac{dP_n}{dt} = k_p (P_{n-1} - P_n) M_\mu - k_{tM} P_n M_\mu - k_{t\beta} P_n - k_d P_n \quad n \geq 2 \quad (15)$$

$$\frac{dM_n}{dt} = k_d P_n + k_{t\beta} P_n + k_{tM} P_n M_\mu \quad n \geq 2 \quad (16)$$

$$\frac{d\lambda_{po}}{dt} = k_p C * M_\mu - k_{t\beta} \lambda_{po} - k_d \lambda_{po} \quad (17)$$

$$\frac{d\lambda_{Mo}}{dt} = k_{t\beta} \lambda_{po} + k_d \lambda_{po} + k_{tM} \lambda_{po} M_\mu \quad (18)$$

$$\frac{d\lambda_{p1}}{dt} = k_p C * M_\mu + k_p \lambda_{po} M_\mu + k_{tM} M_\mu (\lambda_{po} - \lambda_{p1}) - k_{t\beta} \lambda_{p1} - k_d \lambda_{p1} \quad (19)$$

$$\frac{d\lambda_{M1}}{dt} = k_{t\beta} \lambda_{p1} + k_d \lambda_{p1} + k_{tM} \lambda_{p1} M_\mu \quad (20)$$

$$\frac{d\lambda_{p2}}{dt} = k_p C * M_\mu + k_p M_\mu (2\lambda_{p1} + \lambda_{po}) + k_{tM} M_\mu (\lambda_{po} - \lambda_{p2}) - k_{t\beta} \lambda_{p2} - k_d \lambda_{p2} \quad (21)$$

$$\frac{d\lambda_{M2}}{dt} = k_{t\beta} \lambda_{p2} + k_d \lambda_{p2} + k_{tM} \lambda_{p2} M_\mu \quad (22)$$

The kth moments of live and dead polymers are defined as:

$$\lambda_{pk} = \sum_{n=1}^{\infty} n^k [P_n] \quad (23)$$

$$\lambda_{Mk} = \sum_{n=1}^{\infty} n^k [M_n] \quad (24)$$

Where [P] is the total live polymer concentration and $[P]=\lambda_{Po}$.

The Number and weight average molecular weight are calculated using the following equations:

$$M_n = \left[\frac{\lambda_{p1} + \lambda_{M1}}{\lambda_{po} + \lambda_{Mo}}\right] (mw)_{sty} \quad (25)$$

$$M_w = \left[\frac{\lambda_{p2} + \lambda_{M2}}{\lambda_{p1} + \lambda_{M1}}\right] (mw)_{sty} \quad (26)$$

And the poly dispersity index PID is given by:

$$PDI = \frac{M_w}{M_n} \quad (27)$$

Where $(mw)_{sty}$ represents the molecular weight of styrene monomer. In the kinetics model; it is assumed that the catalyst is a single site and is in the first order deactivation. The number and weight average molecular weights and PDI of the polymer in the *i*th shell are obtained by using:

$$M_{n,i} = \left[\frac{\lambda_{p1} + \lambda_{M1}}{\lambda_{po} + \lambda_{Mo}}\right]_i (mw)_{sty} \quad (28)$$

$$M_{w,i} = \left[\frac{\lambda_{p2} + \lambda_{M2}}{\lambda_{p1} + \lambda_{M1}}\right]_i (mw)_{sty} \quad (29)$$

$$PDI_i = \frac{M_{w,i}}{M_{n,i}} \quad i = 1, 2, \ldots\ldots N+1 \quad (30)$$

This model was implemented by using Matlab M—Function program and was solved with a sub routine called ODE15S, which is usually used with stiff differential equations. In Fig. 3, the details of the algorithm of computer

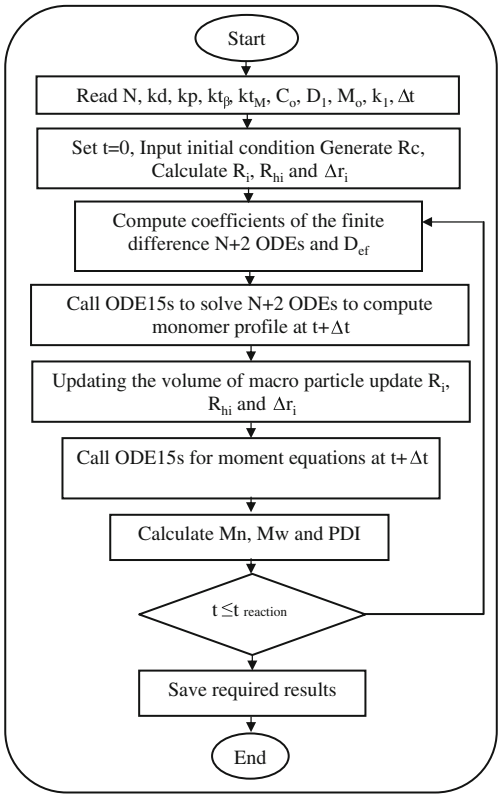


**Fig. 3** Algorithm of computer simulation program

simulation program are presented with all the related equations that are used in this model.

## Results and discussion

The results obtained from this model can be divided in two sections. The first section studies the effects of mass transfer on the rate of polymerization. The second section studies the conduct of (MWD) during the syndiospecific polymerization of styrene over silica-supported catalyst. The set of realistic values of kinetic and physical parameter are taken from experimental studies [26], as shown in Table 1.

### Mass transfer and catalyst particle size effects

In the large particle of high activity catalyst and pores of growing polymer particle, the influence of intraparticle mass transfer will be most pronounced. There is also mass transfer resistance in the microparticles semicrystalline polymer. The mass transfer resistance as a reaction rate will decrease by time; such an increase leads the polymer layer around the catalyst active sites to be thick. Floyd [14–16], focused on the point that in spite of the fact that microparticle diffusion resistance should be taken into account in some cases, especially, with catalyst poor break up, the diffusion resistance in macroparticle pores remains the most influential one; a matter that will be concentrated on in the current paper.

This model solves the macroparticle and microparticle monomer concentration profile based on combining features of MGM and PMGM. The general result that has been arrived at is that this model is used to study the effects of different parameters, such as the time of polymerization,

**Table 1** Reference values of parameters for simulation of syndiospecific polystyrene [26]

| Parameter | Value | Unit |
|---|---|---|
| $M_b$ | 3.24 | mol .$L^{-1}$ |
| C* | $2.62*10^{-4}$ | mol .$L^{-1}$ |
| $R_c$ | 10–50 | μm |
| $R_o$ | 50–150 | μm |
| $D_1$ | $1*10^{-8}$ | $cm^2.min^{-1}$ |
| $D_s$ | $1*10^{-7}$ | $cm^2.min^{-1}$ |
| R | 1.987 | cal.$mol^{-1}$ $K^{-1}$ |
| T | 343 | K |
| $(mw)_{sty}$ | 104.14 | gm.$mol^{-1}$ |
| kd | 1.67 | $hr^{-1}$ |
| kp | 8150 | L. $mol^{-1}$ .$hr^{-1}$ |
| $k_{t\beta}$ | 7.81 | $hr^{-1}$ |
| $k_{tM}$ | 3.11 | L. $mol^{-1}$ .$hr^{-1}$ |

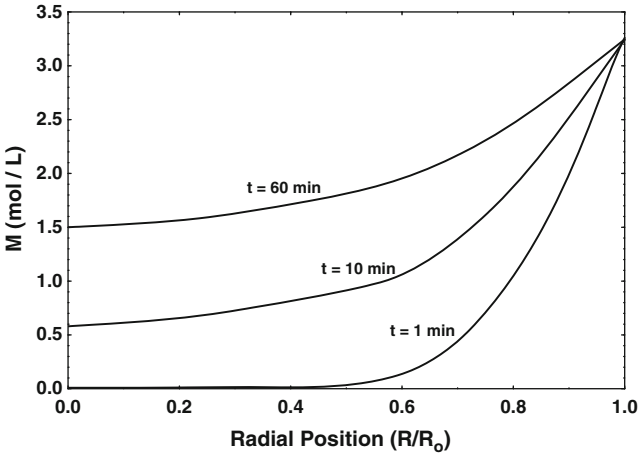


**Fig. 4** Profiles of the monomer concentration as a function of radial position within the growing macro particle at different reaction times and $R_c$=10 μm, $D_1=1*10^{-7}$ $m^2$/sec

diffusion resistance (represented by $D_1$), and catalyst particle size ($R_c$) on monomer concentration within the growing macro particle and on the rate of polymerization. Figure 4 shows steeper monomer concentration profiles as a function of the radial growth of the macro particle at different reaction times. From this figure, it is noticed that the distribution curves of monomer concentration within macro particle growing are present in the first minutes of the reaction. This is because at the beginning of polymerization, the reaction rate is at its maximum while the exposed area of the source monomer is at its minimum.

Furthermore, the impact of the diffusion resistance in the macro molecules in return affects the rate of catalyst decay by increasing the penetration of monomer molecules under the influence of diffusion. Figure 5 shows the curves of polymerization rate at varying degrees of macroparticle diffusion resistance. From this figure, it is clearly noticed

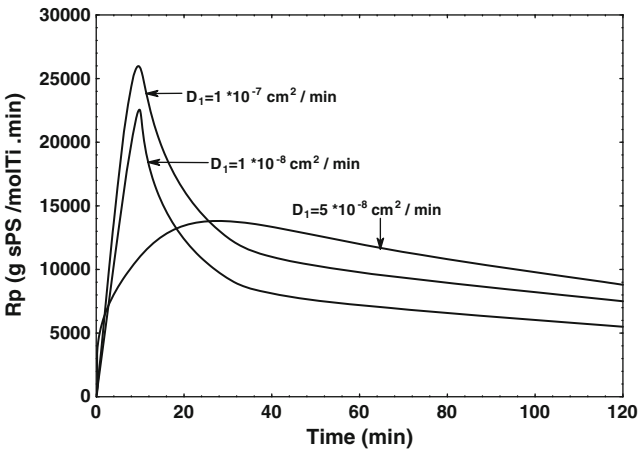


**Fig. 5** Rate of polymerization with varying degree of macroparticle diffusion resistance and $R_c$=10 μm

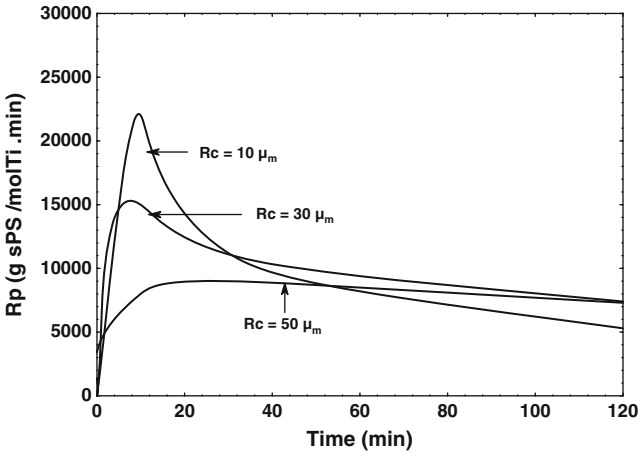


**Fig. 6** Rate of polymerization over different Catalyst particle size ($R_c$) and $D_1=1*10^{-8}$ $cm^2/sec$

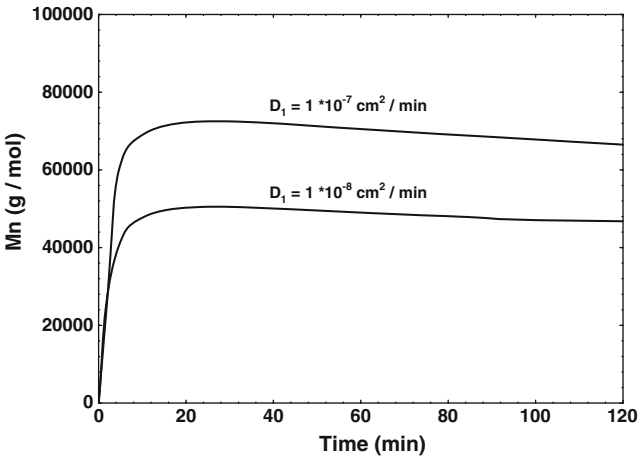


**Fig. 8** Number average molecular weight with varying degree of macroparticle diffusion resistance and $R_c=50$ μm

that the diffusion resistance is more intense in the beginning of polymerization reaction; however, it decreases with increasing the size of polymer particles. This gives an interesting and accurate effect to some extent.

It is beneficial to study the influence of catalyst properties, like that of particle size on the dynamic process of particles growth. Figure 6 shows the rates of polymerization at varying catalyst particle size ($R_c$). From this figure, it is illustrated that increasing the size of the catalyst particles leads to a decrease in the rate of polymerization due to the increased rate of the monomer consumption.

## Molecular weight and molecular weight distribution

In this portion, the simulation of (MWD) over styrene polymerization will be present. As it is said previously, the molecular weight and the poly dispersity index (PDI) can be calculated from the zeroth, first and second moments.

With the development of catalysts, the rate of chain transfer becomes very fast; this makes the molecular weight almost constant within a very short time from the start point of polymerization process. Figure 7 shows a number of average molecular weights over different particle sizes of the catalyst, in addition to the constant diffusion limitation. It has been seen from this figure that the influence of the volume catalyst particles on the molecular weight is fewer.

For deactivating the catalyst in the present of diffusion restrictions, consider Fig. 8, which shows a number of average molecular weights with varying degrees of macroparticle diffusion resistance; in addition to the constant particle size of the catalyst. From this figure, it has been noticed that the molecular weight increases with time because the deactivation of catalyst leads to an increase in the concentration of monomer in the particle, and hence, to an increase in the molecular weight with the passage of time.

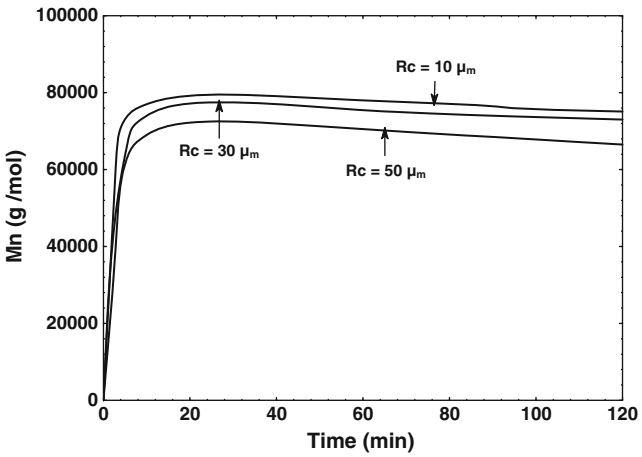


**Fig. 7** Number average molecular weight over different catalyst particle size ($R_c$) and $D_1=1*10^{-7}$ $m^2/sec$

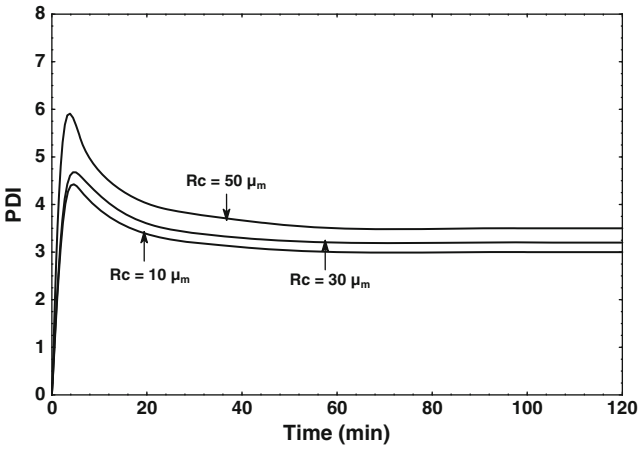


**Fig. 9** PDI over different catalyst Particle size ($R_c$) and $D_1=1*10^{-7}$ $m^2/sec$

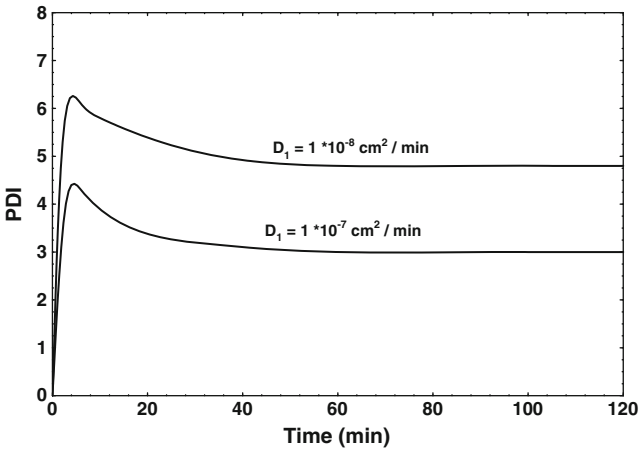


**Fig. 10** Polydispersity index with varying degree of macroparticle diffusion resistance and $R_c$=10 μm

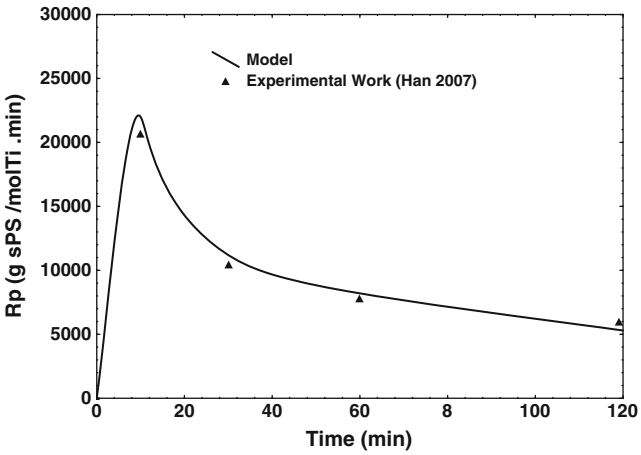


**Fig. 11** Rate of polymerization predicted by model and experimental work (Han 2007) ($R_c$=10 μm, $D_1$=1*10$^{-8}$ cm$^2$/min, Mo=3.24 mol/L, C*=2.62*10$^{-4}$ mol/L, T=343 K)

One of the biggest secrets in the polymerization using catalyst is the increase in the polydispersity index (PDI) that is generally observed. This increase usually does not exceeding two (PDI=2) from the standard kinetic mechanism. According to the hypothesis, and with respect to the existence of mass transfer resistance and the effect of catalyst particles size, it was observed a variation in the concentration of monomer particles on the surface of the catalyst particles. However, such a variation in the concentration is higher in the outer regions than in the interior regions of these particles. As a result, the polymer produced has different molecular weights; a state that helps gives a large PDI. In this model and when assuming the catalyst particles that contain a single active site, large PDI were noticed in the first minutes of polymerization, as shown in Figs. 9 and 10.

## Model validation

The simulation results obtained from this model have been validated with experimental data proposed by Han et al. [26], the authors study the experimental analysis of a slurry phase sPS polymerization over silica-supported Cp*Ti (OCH3)3/MAO catalyst.

According to Han et al. [26], the polymerization experiments were carried out using a 100 mL jacketed glass reactor equipped with a stainless steel agitator. Predetermined amounts of monomer, solvent, silica-supported catalyst, and MAO were charged into the reactor in a glove box. All the polymerization experiments were carried out at 70 °C. After polymerization, the reaction mixture washed with excess amount of acidified methanol and dried in vacuo. Since the reactor has no provisions for sampling during the polymerization, the polymer yield vs. time profiles were obtained by conducting the individual experiments with same reaction conditions but terminated at different reaction times. For each polymerization experiment, monomer conversions and remained monomer concentrations were calculated from polymer yield data. The polymerization rate values were determined by averaging the slopes of two adjacent points for each data point with ORIGIN package (Origin Lab, Ver. 7.5).The number and weight average molecular weight were determined by gel permeation chromatography (GPC). Table 2 shows some of experimental results for the sPS polymerization, which were obtained from the Han et al.[26], and used to validate our model. Figure 11 show that the comparison between simulated results obtained by our model and experimental work of Han et al.[26], for rate of polymerization at ($R_c$=10 μm and $D_1$=1*10$^{-8}$ cm$^2$/min), from this Figure it is clearly the results given a good agreement.

The results of number average molecular weight predicted by our model with experimental data shown in Fig. 12, the Figure give agreement with the experimental work within a confidence interval of±5%.

**Table 2** Experimental data of sPS polymerization with silica-supported metallocene catalyst

| Run | $[M]_{bo}$ [mol /L] | $[Ti]\times10^4$ [mol /L] | Styrene [Vol.%] | Time [min] | Yield [g] | Avg. activity$\times10^{-3}$ [g sPS/mol Ti min] | Mw$\times10^{-5}$ [g/mol] | PDI [–] |
|---|---|---|---|---|---|---|---|---|
| 1 | 3.24 | 2.62 | 40 | 10 | 3.49 | 20.65 | 2.65 | 3.74 |
| 2 | | | | 30 | 5.30 | 10.45 | 2.42 | 3.04 |
| 3 | | | | 60 | 7.92 | 7.81 | 2.21 | 3.24 |
| 4 | | | | 120 | 12.14 | 5.99 | 2.39 | 3.71 |

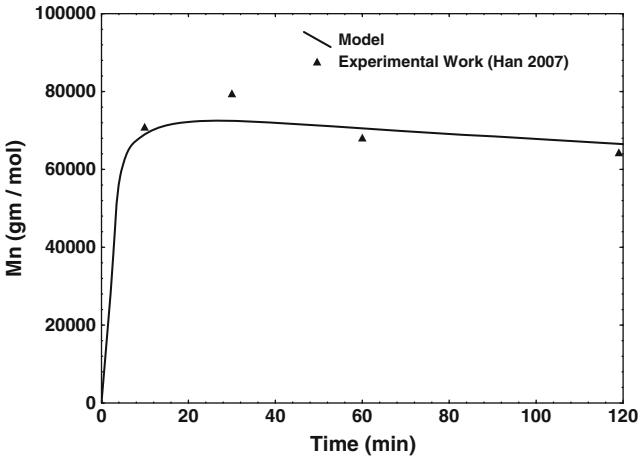


**Fig. 12** Number average molecular weight predicted by model and experimental work. ($R_c$=50 μm, $D_1$=1*10$^{-7}$ cm$^2$/min, Mo=3.24 mol/L, C*=2.62*10$^{-4}$ mol/L, T=343 K)

Figure 13 show that the results of PDI validated with experimental data [26], from this figure it is pronounced the (PDI) at ($R_c$=10 μm and $D_1$=1*10$^{-7}$ cm$^2$/min) given agreement with experimental work [26].

## Conclusions

A comprehensive mathematical model for syndiospecific styrene polymerization based on combining features from the MGM and PMGM has been presented and used. The purpose of this model is to simulate the effects of intra-particle mass transfer on polymerization behavior for syndiospecific styrene system. From the results above, one can conclude, the degree of diffusion resistance is dependent on the physical properties of the catalyst and the effects of the polymerization rate are more strongly than that of the polymer properties.

Moreover, the validation of the model with experimental data [26], given a good agreement results and show that the model is able to predict a correct monomer concentration profile in each macro and micro particle, polymerization rate, particle growth factor and the most important polymer properties represented by the molecular weight and MWD.

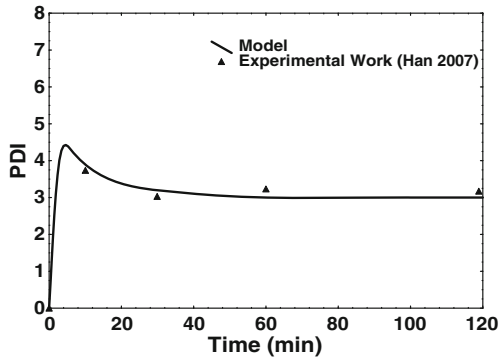


**Fig. 13** PDI predicted by model and experimental work (Han 2007) ($R_c$=10 μm, $D_1$=1*10$^{-7}$ cm$^2$/min, Mo=3.24 mol/L, C*=2.62*10$^{-4}$ mol/L, T=343 K)

**Acknowledgments** The authors gratefully acknowledge the Universiti Sains Malaysia (USM) for supporting this work under (USM) Fellowship.

## Appendix 1

The changes in the shells volume, $\Delta V_i$ and the location of the grid points $R_i$ with time are given in this section. As show in Fig. 2, the hypothetical shell can be defined as $R_{h,i-1} \le r \le R_{h,i}$ such that the entire polymer produced by the catalyst particles of radius $R_c$ are accommodated in it . In the interval t to t+Δt, the total volume of polymer and the volume of micro particle produced at ith shell are given by:

$$\frac{dV_i}{dt} = \frac{0.001\, k_p C^* M_{\mu,i+1} \left(N_i \frac{4}{3}\pi R_c^3\right) mw_{sty}}{\rho_p} \tag{1.1}$$

$$\frac{dV_{s,i}}{dt} = \frac{0.001\, k_p C^* M_{\mu,i} \left(\frac{4}{3}\pi R_c^3\right) mw_{sty}}{\rho_p} \tag{1.2}$$

With $V_i(t=0)$ and $V_{S,i}(t=0)$ being the initial total volume and volume of every polymer micro particle of ith volume, respectively.

$$V_i(t=0) = \frac{N_i \left(\frac{4}{3}\pi R_c^3\right)}{1-\varepsilon} \tag{1.3}$$

$$V_{s,i}(t=0) = \frac{4}{3}\pi R_c^3 \tag{1.4}$$

We can now define the hypothetical shells at any time by:

$$R_{h,i} = \left(\frac{3}{4\pi}\sum_{j=1}^{i} V_j\right)^{1/3} \tag{1.5}$$

Where $R_{h,o}$=0 and the radius of micro particle at ith shell being:

$$R_{s,i} = \left(\frac{3}{4\pi} V_{s,i}\right)^{\frac{1}{3}} \tag{1.6}$$

The catalyst particles are assumed to be placed at the mid points of each hypothetical shell. Thus:

$$R_{1,i} = R_{h,i-1} + \frac{1}{2}\left(R_{h,i} - R_{h,i-1}\right) \tag{1.7}$$

Then the computational grid points are related to $R_{1,i}$ by:

$$R_1 = 0 \tag{1.8}$$

$$R_2 = R_c \tag{1.9}$$

$$R_{i+1} = R_{1,i} + R_{s,i} \tag{1.10}$$

$$R_{N+2} = R_{h,N} \tag{1.11}$$

The values of $\Delta r_i$ to be used in the equation (6a, b & c) are given by:

$$\Delta r_i = R_{i+1} - R_i \tag{1.12}$$

## References


1. Odian GG (2004) Principles of polymerization. Wiley-Interscience, Hoboken
2. Schellenberg J (2010) Syndiotactic polystyrene: synthesis, characterization, processing, and applications. Wiley, Hoboken
3. He F-A, Zhang L-M, Yang F, Chen L-S, Wu Q (2006) New nanocomposites based on syndiotactic polystyrene and organo-modified ZnAl layered double hydroxide. J Polymer Res 13 (6):483–493. doi:10.1007/s10965-006-9071-9
4. Gao Y, Nie Z, Li H (2009) Synthesis of syndiotactic polystyrene-poly(ethylene glycol) copolymer by photochemical reaction. J Polymer Res 16(6):709–717. doi:10.1007/s10965-009-9277-8
5. Gao Y, Li H-M, Liu F-S, Wang X-Y, Shen Z-G (2007) Synthesis and characterization of benzoylated syndiotactic polystyrene. J Polymer Res 14(4):291–296. doi:10.1007/s10965-007-9109-7
6. Ishihara N, Seimiya T, Kuramoto M, Uoi M (1986) Crystalline syndiotactic polystyrene. Macromolecules 19(9):2464–2465. doi:10.1021/ma00163a027
7. Ghosh S (2009) Influence of cocatalyst on the stereoselectivity and productivity of styrene polymerization reactions. J Polymer Res 16 (2):117–124. doi:10.1007/s10965-008-9209-z
8. Schmeal WR, Street JR (1971) Polymerization in expanding catalyst particles. AIChE J 17(5):1188–1197. doi:10.1002/aic.690170526
9. Schmeal WR, Street JR (1972) Polymerization in catalyst particles: calculation of molecular weight distribution. J Polymer Sci: Polym Phys Ed 10(11):2173–2187. doi:10.1002/pol.1972.180101106
10. Nagel EJ, Kirillov VA, Ray WH (1980) Prediction of molecular weight distributions for high-density polyolefins. Ind Eng Chem Prod Res Dev 19(3):372–379. doi:10.1021/i360075a016
11. Singh D, Merrill RP (1971) Molecular weight distribution of polyethylene produced by Ziegler-Natta Catalysts. Macromolecules 4(5):599–604. doi:10.1021/ma60023a017
12. Galvan R, Tirrell M (1986) Orthogonal collocation applied to analysis of heterogeneous Ziegler-Natta polymerization. Comput Chem Eng 10(1):77–85
13. Galvan R, Tirrell M (1986) Molecular weight distribution predictions for heterogeneous Ziegler-Natta polymerization using a two-site model. Chem Eng Sci 41(9):2385–2393
14. Floyd S, Choi KY, Taylor TW, Ray WH (1986) Polymerization of olefins through heterogeneous catalysis. III. Polymer particle modelling with an analysis of intraparticle heat and mass transfer effects. J Appl Polym Sci 32(1):2935–2960. doi:10.1002/app.1986.070320108
15. Floyd S, Choi KY, Taylor TW, Ray WH (1986) Polymerization of olefines through heterogeneous catalysis IV. Modeling of heat and mass transfer resistance in the polymer particle boundary layer. J Appl Polym Sci 31(7):2231–2265. doi:10.1002/app.1986.070310724
16. Floyd S, Hutchinson RA, Ray WH (1986) Polymerization of olefins through heterogeneous catalysis—V. Gas-liquid mass transfer limitations in liquid slurry reactors. J Appl Polym Sci 32 (6):5451–5479. doi:10.1002/app.1986.070320617
17. Hutchinson RA, Chen CM, Ray WH (1992) Polymerization of olefins through heterogeneous catalysis X: modeling of particle growth and morphology. J Appl Polymer Sci 44(8):1389–1414. doi:10.1002/app.1992.070440811
18. Sarkar P, Gupta SK (1991) Modelling of propylene polymerization in an isothermal slurry reactor. Polymer 32(15):2842–2852
19. Sarkar P, Gupta SK (1992) Simulation of propylene polymerization: an efficient algorithm. Polymer 33(7):1477–1485
20. Soares BPJ, Hamielec EA (1995) General dynamic mathematical modelling of heterogeneous Ziegler-Natta and metallocene catalyzed copolymerization with multiple site types and mass and heat transfer resistances, vol 3. vol 3. Dekker, New York, NY, ETATS-UNIS.
21. Kanellopoulos V, Dompazis G, Gustafsson B, Kiparissides C (2004) Comprehensive analysis of single-particle growth in heterogeneous olefin polymerization: the random-pore polymeric flow model. Ind Eng Chem Res 43(17):5166–5180. doi:10.1021/ie030810u
22. Chen Y, Liu X (2005) Modeling mass transport of propylene polymerization on Ziegler-Natta catalyst. Polymer 46(22):9434–9442
23. Liu X (2007) Modeling and simulation of heterogeneous catalyzed propylene polymerization. Chin J Chem Eng 15(4):545–553
24. Kanellopoulos V, Tsiliopoulou E, Dompazis G, Touloupides V, Kiparissides C (2007) Evaluation of the internal particle morphology in catalytic gas-phase olefin polymerization reactors. Ind Eng Chem Res 46(7):1928–1937. doi:10.1021/ie060721s
25. Finlayson BA (1980) Nonlinear analysis in chemical engineering. McGraw-Hill International Book Co.,
26. Han JJ, Lee HW, Yoon WJ, Choi KY (2007) Rate and molecular weight distribution modeling of syndiospecific styrene polymerization over silica-supported metallocene catalyst. Polymer 48 (22):6519–6531